

GT2011-4* +%

TURBINE HUB AND SHROUD SEALING FLOW LOSS MECHANISMS

Metodi Blagoev Zlatinov *
Choon Sooi Tan

Gas Turbine Laboratory
Massachusetts Institute of Technology
Email: zlatinov@mit.edu

Matthew Montgomery
Tito Islam
Melissa Seco-Soley

Gas Turbine Engineering
Siemens Energy Inc.
Orlando, Florida

ABSTRACT

Purge air is injected through seals in the hub and shroud of axial turbines in order to prevent hot gas ingestion into the inter-stage gaps. An investigation into the losses involved with the injection of purge air has been undertaken, with the objectives of answering where the losses are generated, how they are generated, and what are the most effective ways for reducing them. In order to address these questions, a consistent framework for interpreting entropy generation as a measure of loss is developed for turbomachinery applications with secondary air streams. A procedure for factoring out distinct effects is also presented. These tools, applied to steady computations, elucidate four routes through which change in loss generation is brought about by injection of purge air: a shear layer between purge and main streams, interaction with the passage vortex system that generates radial velocity gradients, changes in wetted loss and tip clearance flow due to an increased degree of reaction, and the potential for reducing tip clearance flow for the case of purge flow injected from the shroud. An emphasis is placed on tracing these effects to specific purge flow characteristics that drive them. The understanding gained provides a rationale for the observed sensitivity of purge flow losses to the design parameters purge air mass fraction and swirl, compared to purge slot axial inclination and gap width. Pre-swirling of purge flow is less effective in mitigating losses in the case of shroud-injection, since there is a tradeoff with the tip clearance flow suppression effect.

NOMENCLATURE

\mathcal{A} Area
 c_x Axial chord
 d_g Purge gap width
 h Specific enthalpy
 k_{eff} Effective thermal conductivity
 \dot{m} Mass flow rate
 μ_{eff} Effective viscosity
 Ω Angular speed
 P Pressure
 q_{in} Heat transfer per unit area into control volume
 r_{hub} Hub radius
 s Specific entropy
 \dot{S}_{gen}''' Entropy generation rate per unit volume
 T Temperature
 τ_{ij} Shear stress tensor
 U Disk rim speed, $U = \Omega r_{hub}$
 V Velocity
 \mathcal{V} Volume
 w Specific work

Subscripts and Superscripts

a,b Primary and secondary streams
 ma Mass-averaged quantity
 R_{in} Rotor inlet plane
 rel Relative frame
s,c,r Streamwise, cross-flow and radial directions

* Address all correspondence to this author.

TE Rotor trailing edge plane
 tot Sum of all streams
 t1,t2 Stagnation quantity at inflow and outflow
 t2s Stagnation quantity after ideal expansion
 therm Due to heat transfer
 visc Due to viscous effects
 wa Work-averaged quantity
 x,θ,r Axial, circumferential and radial directions

Non-Dimensional Quantities

AR Aspect Ratio
 η Efficiency
 gf Gap fraction, $\frac{d_g}{(r_{tip}-r_{hub})}$
 λ degree of reaction, $\frac{\Delta h_{rotor}}{\Delta h_{stage}}$
 mf Mass fraction, $\frac{m_b}{m_a}$
 M Mach number
 π Stage pressure ratio
 Ψ Stage Loading, $\frac{\Delta h_t}{(\Omega r_{midspan})^2}$
 Φ Flow Coefficient, $\frac{V_x}{\Omega r_{midspan}}$
 φ Injection angle
 sf Swirl fraction, $\frac{V_\theta}{U}$
 σ Solidity, (chord length/pitch)

INTRODUCTION

In gas turbines for power generation and aircraft propulsion, sealing air, commonly referred to as purge air, must be ejected through inter-stage gaps in the hub and shroud of axial turbines to prevent hot gas ingestion into the cavities outside the mainstream flow path. These secondary air streams interact with the mainstream flow to generate loss. While it has been demonstrated that certain injection schemes can lead to a reduction in purge flow-related losses, the flow processes that underlie the observed improvements are not well understood. The overall goal of this paper is to delineate and quantify the various loss mechanisms associated with purge flow injection and trace them back to the specific purge flow characteristics, thereby providing guidelines for a design process based on physical rationale.

The existing literature on this subject has been helpful in guiding the research leading to the results in this paper. Pau et. al. [1] found that injecting purge flow leads to an increase in efficiency, mainly due to the modification of the shock system downstream of the stator and to a reduction of the stator trailing edge shock losses. However most studies show efficiency penalties associated with purge flow injection. Kost and Nicklas [2] noted the potential for increasing the horseshoe vortex if the purge slot traverses the saddle point. Reid et. al. [3] conducted measurements and calculations of purge-mainstream interactions, suggesting two loss mechanisms: one due to the mixing of the sealant flow with the mainstream flow and the other

due to the change in the flow through a downstream blade row. However these two mechanisms were not rigorously isolated and quantified in terms of purge flow parameters. Ong et. al. [4] uses an analytical mixing model to isolate the purge-mainstream mixing loss, and links the additional losses to a change in flow angles. More recently, Popovic and Hodson [5] have identified three regimes for loss depending on purge mass flow rate and sealing effectiveness. Some new vortical structures have been observed [6] to emerge from a purge slot on a linear cascade, and have been suggested as a cause of enhanced losses. In terms of design improvements, a number of publications [3] [7] [5] have pointed to the potential for reducing losses through swirling of purge flow prior to injection. McLean et. al. [8] studied three types of injection configurations, and actually observed an increase in efficiency from purge injection via root injection.

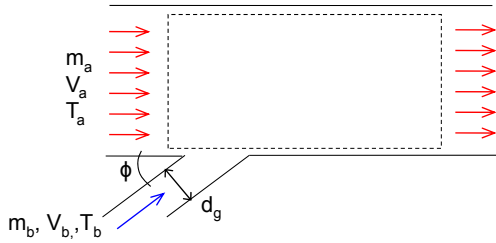
Clearly, a substantial amount of research has been done on secondary air losses. However, a lack of clarity in the causal relationship between these losses and their drivers still prevents a systematic approach to the design of purge flow injection systems. The specific objectives of this paper are to identify where and how additional losses are generated due to purge flow injection, and based on this understanding to propose guidelines as to which design parameters are most effective in mitigating these loss sources. This paper is organized as follows. Framework approach is first described. The results are then presented to first delineate the loss sources in a baseline case with no purge flow. This is followed by results to systematically identify additional loss mechanisms associated with purge flow injection. Finally, a section is devoted to quantitative delineation of design effects.

FRAMEWORK OF RESEARCH APPROACH

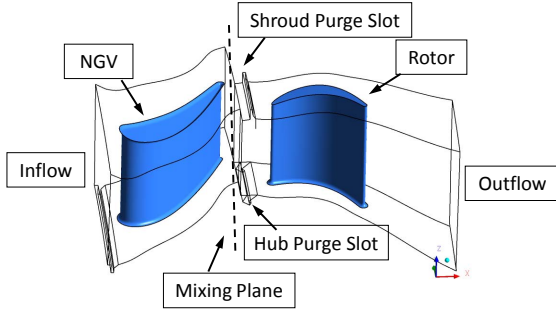
System Modeling

To allow for a systematic delineation of the loss mechanisms associated with purge flow injection, two models of purge flow interacting with mainstream flow have been studied in depth using both analytical and computational tools. The first model, illustrated in Fig. 1(a), consists of purge flow injection into a simple axisymmetric throughflow (an abstraction of a turbine in the form of an annular duct with no blades). The second model consists of a full three dimensional blade passage with nozzle guide vane (NGV) and rotor blade, as depicted in Fig. 1(b). Purge air is injected upstream of the rotor, either at the hub or shroud, and there is a mixing plane upstream of the purge slots. The value of this incremental modeling approach is that it allows for loss mechanisms observed in the axisymmetric configuration to be factored out from the three dimensional configuration, thereby revealing and isolating additional loss mechanisms. The characteristics of the representative first stage high pressure unshrouded turbine used for this investigation are listed in Table 1.

Within this framework, four purge flow parameters were investigated for their effect on loss: the purge air mass flow rate,



(a) axisymmetric model



(b) three dimensional blade passage with mixing plane

FIGURE 1. AXISYMMETRIC AND THREE DIMENSIONAL MODELS

TABLE 1. CHARACTERISTICS OF A REPRESENTATIVE TURBINE STAGE

Quantity	Value	Quantity	Value
Ω	2749 [rad/s]	U	300 [m/s]
AR_{rotor}	1.11	π	0.546
$M_{rotorin}$	0.785	λ	0.412
Ψ	2.17	Φ	0.65
T_{purge}/T_{main}	0.5	σ_{rotor}	1.37

circumferential (swirl) velocity of purge flow prior to injection, purge jet axial inclination and purge gap width (the last two parameters control purge flow axial and radial momentum, for a given purge mass flow rate). These design parameters are cast in non-dimensional terms as the purge flow mass fraction (mf), swirl fraction of the rim speed (sf), injection angle (ϕ) and gap fraction of the annulus height (gf). The design space for which this investigation was performed was chosen to be a superset of the typical range of parameter values found in industry, spanning $0 < sf < 1$, $0 < mf < 0.015$, $0 < \phi < 90^\circ$, $0.05 < gf < 0.083$.

Computational and Analytical Tools

The axisymmetric model was investigated both analytically, based on the method outlined in [9], and computationally, using the Ansys 12.0 CFX solver on a structured grid. The three dimensional blade passage was investigated computationally, with structured grids generated with the default topology of AutoGrid - O4H¹. Grid-convergence studies showed that increasing the number of nodes used for modeling from 0.9 to 1.9 million results in only 3% change in the total losses and less than 1% change in net purge flow losses. Most of the results presented are from the finer mesh, while the coarse mesh was used for more expedient parametric studies. In all computations the $k - \omega$ Shear Stress Transport turbulence model was used with wall functions ($y^+ \approx 12$). A typical turbulence intensity of 10% was imposed at the NGV inlet boundary and 5% at the purge slot inlet boundary.

Interpretation of Entropy as a Measure of Loss

Entropy generation due to irreversible processes can be related to lost opportunity to do work in a turbine through the arguments in Appendix A. It will also be shown in the following subsection that volumetric entropy generation rate can be a useful tool for tracing losses to responsible flow features. For these reasons the authors have chosen to use entropy generation as the measure of loss. However, it is important to realize that entropy generation due to thermal mixing is not a loss with respect to the turbine but rather to the cycle, and in assessing turbine performance one must consider viscous effects only. This section presents a method for isolating viscous losses in the context of multi-stream and non-uniform flow expansion.

Consider first the scenario of multiple streams of working fluid with distinct inlet conditions being expanded through a turbine to the same downstream stagnation pressure. One way of dealing with such an expansion is by tracing each individual fluid stream as it expands through the turbine, but a much more practical approach is illustrated in Fig. 2 for the case of two streams, a and b. The first step is to replace the non-uniform inlet flow with an equivalent uniform flow that would produce the same work output if expanded through a turbine. To obtain an appropriate average stagnation pressure, consider the thought experiment in which the higher pressure stream is expanded isentropically to a pressure P_{11}^{wa} such that the work output from this process is just enough to compress the lower pressure stream to the same P_{11}^{wa} . This process generates no net work, and essentially describes the useful concept of “work-averaging” developed in [10]. Work-averaged pressure is applicable not only for dealing with multiple discrete streams but also with continuous non-uniformities in stagnation pressure and will be used extensively throughout this paper. The expression for work-averaged pressure, derived

¹refer to NUMECA AutoGrid5 user manual

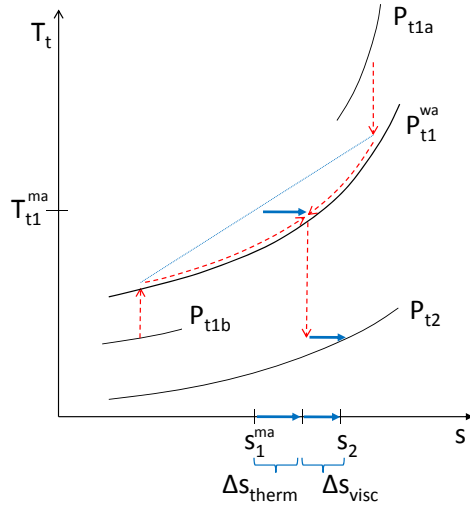


FIGURE 2. T-S DIAGRAM OF MULTI-STREAM EXPANSION.

in [10], is therefore reproduced here in Eqn. (1)

$$P_t^{wa} = \left[\frac{\int T_t d\dot{m}}{\int T_t / P_t^{\frac{\gamma-1}{\gamma}} d\dot{m}} \right]^{\frac{\gamma}{\gamma-1}} \quad (1)$$

Returning to the simple example of two discrete streams, mass flow averaging of stagnation temperature allows us to fix the state of the substitute uniform flow, while enforcing energy conservation. Expanding this hypothetical uniform flow, with inlet conditions P_{t1}^{wa} and T_{t1}^{ma} , to any downstream pressure will yield the same work output as if the two original streams were expanded independently to that same downstream pressure. The “ideal” work output of these two streams is therefore readily given by Eqn. (2).

$$w_{ideal} = c_p T_{t1}^{ma} \left[1 - \left(\frac{P_{t2}^{wa}}{P_{t1}^{wa}} \right)^{\frac{\gamma-1}{\gamma}} \right] \quad (2)$$

However, the qualifier “ideal” has been put in quotations because mass flow averaging of stagnation temperature amounts to thermal mixing at constant pressure. This process is irreversible and generates an amount of entropy Δs_{therm} , as indicated in Fig. 2. Theoretically, a heat engine, such as the one discussed in [11], could have been used to bring the two streams into thermal equilibrium reversibly, generating additional work amounting to $\tilde{T}_{t2} \Delta s_{therm}$ (The reference temperature $\tilde{T}_{t2} \approx T_{t2}$ is discussed in Appendix A). In practice, this cannot be accomplished with a simple turbine, and the thermal mixing loss is

unavoidable. Therefore, as far as a turbine component is concerned, w_{ideal} alone is the relevant ideal work. The irreversible thermal mixing that generates Δs_{therm} is not a debit to turbine performance but rather a cycle loss that will be accounted for most rigorously through cycle analysis, as shown in [12] [13].

In an expansion process through a non-ideal turbine entropy will also be generated due to viscous effects, Δs_{visc} , with attendant lost opportunity to do work given by Eqn. (3).

$$\begin{aligned} w_{visc\ loss} &= \tilde{T}_{t2} \Delta s_{visc} = \tilde{T}_{t2} (\Delta s - \Delta s_{therm}) = w_{ideal} - w_{actual} \\ &= c_p \left[T_{t2}^{ma} - T_{t1}^{ma} \left(\frac{P_{t2}^{wa}}{P_{t1}^{wa}} \right)^{\frac{\gamma-1}{\gamma}} \right] \end{aligned} \quad (3)$$

It is only these viscous losses that are of interest to the turbine designer, and it is crucial that entropy generated by viscous effects is isolated from total entropy generated. For steady flows, Eqn. (3) provides a convenient way of doing this with work-averaged stagnation pressure and mass-averaged stagnation temperature.

Estimates of Viscous Entropy Generation

For the axisymmetric configuration in Fig. 1(a), the entropy generation due to viscous effects can be estimated analytically using the control volume mixed out approach outlined by Young and Wilcock [9]. The only modification made to Young and Wilcock’s analysis is the incorporation of circumferential velocity, resulting in Eqn. (4). The quantities in this equation can be expressed in terms of the non-dimensional purge flow parameters under investigation, allowing for an expedient parametric study of their effects on loss.

$$\Delta s_{visc} = \frac{m_b}{m_a} \left[\frac{(V_{x,a} - V_{x,b})^2 + (V_{r,a} - V_{r,b})^2 + (V_{\theta,a} - V_{\theta,b})^2}{2T_a} \right] \quad (4)$$

The accumulation of actual viscous losses up to any given axial location (as opposed to the fully mixed out loss) can be extracted from the CFD solution and plotted as a function of axial distance, as in Fig. (3). This is done by applying Eqn. (3) between appropriately averaged inlet conditions (pressure being work-averaged and temperature mass-averaged) and similarly averaged outflow conditions at consecutive axial cuts through the computational domain. Plotting accumulated viscous losses as a function of distance through the axisymmetric duct or three dimensional blade passage provides quantitative insight into the distribution of loss sources in the axial dimension.

Further insight into the spatial distribution of entropy sources can be gained from the quantity “entropy generation rate per unit volume”. Consider the formulation of a steady state conservation equation for entropy consisting of convection, diffusion

and source terms, as per Eqn. (5)

$$\iint_{\mathcal{A}} \rho s \vec{V} \cdot d\vec{\mathcal{A}} - \iint_{\mathcal{A}} \frac{q_{in}}{T} d\mathcal{A} = \iiint_{\mathcal{V}} \dot{S}_{gen}''' d\mathcal{V} \quad (5)$$

By construction, the left-hand-side of Eqn. (5) gives the rate at which entropy is generated inside a given control volume (the difference between entropy flowing in and out, minus any changes associated with reversible heat transfer). It can be shown [14] that the volumetric source term on the right-hand-side, \dot{S}_{gen}''' , is the sum of two components - viscous and thermal dissipation, which are given by equations (6) and (7) respectively

$$\dot{S}_{visc}''' = \frac{1}{T} \tau_{ij} \frac{\partial u_i}{\partial x_j} \quad (6)$$

$$\dot{S}_{therm}''' = \frac{k_{eff}}{T^2} \left(\frac{\partial T}{\partial x_j} \right)^2 \quad (7)$$

Contours of \dot{S}_{visc}''' in particular provide a useful tool for establishing traceability between turbine losses and flow features. However, it is important to consider that direct numerical evaluation of entropy generation rates via equations (6) and (7) is challenging due to the quadratic dependence on velocity and temperature gradients. As mentioned earlier, increasing the number of nodes used for modeling the three dimensional blade passage from 0.9 to 1.9 million has little effect (3% change in the total losses and less than 1% change in net purge flow losses) on the result obtained using the left-hand-side of Eqn. (5), indicating grid convergence. On the other hand, the right-hand-side estimates losses 53% lower for the coarse grid and 41% lower for the fine grid. Further grid refinement studies on the axisymmetric configuration (Fig. 1(a)) demonstrated that the right-hand-side does indeed converge to the numerically correct value of dissipation, but only for extremely high grid densities that are impractical in three dimensions (particularly due to the secondary flows that introduce regions of high gradients away from the relatively well resolved endwall region). Nevertheless, though the volume integral of entropy generation rate underestimates losses, this is largely a systematic error, since the *distribution* of accumulated loss as calculated by the two methods was found to be in agreement. Therefore, the authors have used contours of volumetric entropy generation rate as calculated by Eqn. (6) as a qualitative tool for identifying local regions of high loss, while any quantitative conclusions are based on the accumulated loss curves obtained with Eqn. (3) (example: Fig. 3).

RESULTS

Having established a consistent framework for interpreting loss, our key findings, addressing where and how losses are generated will be presented in this section. The losses in the baseline

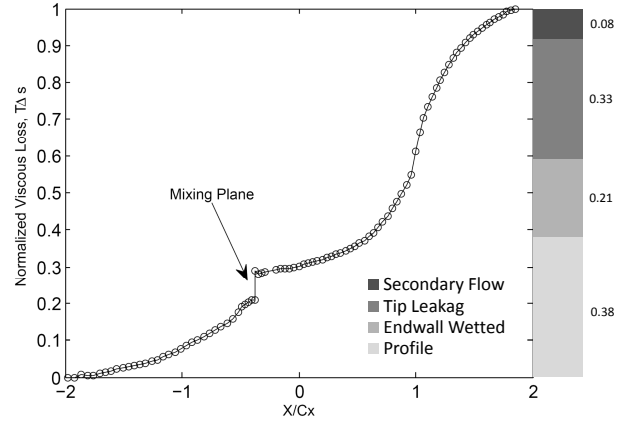


FIGURE 3. ACCUMULATED VISCOUS LOSS FOR BASELINE CASE WITH NO PURGE FLOW

case without purge flow will be presented first, followed by the additional loss mechanisms associated with purge flow injection.

Baseline Losses

The accumulation of viscous loss as a function of axial distance through the blade passage domain is shown in Fig. 3. Loss (ordinate) is normalized by the total loss up to the outflow plane, which is 0.8 axial chord lengths downstream of the rotor trailing edge; the axial distance (abscissa) is measured from the leading edge of the rotor and is normalized by the rotor axial chord, such that the rotor spans 0-1. There is a discrete jump in loss that marks the location of the mixing plane. A breakdown of the total losses into components of profile loss, endwall wetted loss, tip clearance flow loss and secondary flow loss are also presented in Fig. 3. The procedure for delineating the various loss components is outlined in Appendix B. It is clear that most of the losses are generated in the rotor, and that tip clearance flow is a significant contributor.

Further insight into the spatial distribution of loss sources can be gained from Fig. 4, which shows contour plots of \dot{S}_{visc}''' at various streamwise locations of the rotor blade ($X/C_x = 0 - 1.4$). It is clear that the passage vortex system (region A) generates only relatively mild losses. On the other hand, the tip clearance flow vortex begins to dominate as a source of entropy generation beyond 50% axial chord and well downstream of the blade trailing edge (regions B,C)- an observation that is in accord with the steep increase in accumulated loss seen in Fig. 3.

Losses Due to Purge Flow

Having examined the viscous losses in a baseline case with no purge flow, this section discusses the additional losses associated with purge flow injection into the main stream. Four effects are identified and quantified in terms of their drivers: 1) viscous

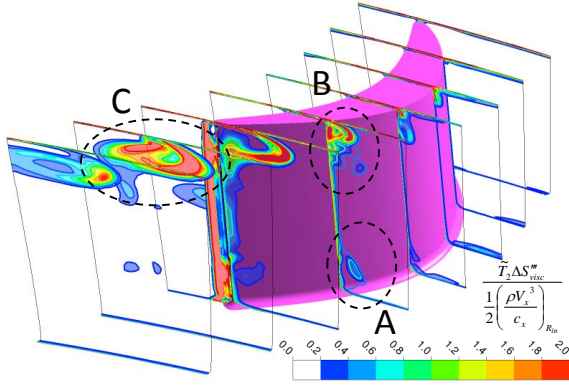


FIGURE 4. ENTROPY GENERATION RATE PER UNIT VOLUME AT AXIAL PLANES THROUGH ROTOR

shear layer, 2) purge flow-passage vortex interaction, 3) losses related to change in reaction and 4) purge-tip clearance flow interaction.

1. Viscous Shear Layer. When purge flow is injected upstream of the rotor, it generally has a velocity deficit with respect to the mainstream flow, particularly in the V_θ component. This generates a shear layer at the interface between the purge and main streams that generates entropy as the velocity gradients are dissipated through viscous action. The phenomenon is observed most clearly in the meridional plane, shown for the axisymmetric and three dimensional configurations in Fig. 5. Note that this is the only viscous loss mechanisms for the axisymmetric configuration (Fig. 1(a)).

Since this shear layer is largely an axisymmetric effect, it is convenient to study the sensitivity of this loss to design parameters using the analytical control volume analysis that yielded Eqn. (4). The results of such an analysis are given in Fig. 6, showing the change in normalized loss ($\tilde{T}_{12} \Delta s_{visc}$ normalize by the baseline losses given in Fig. 3) associated with mixing out purge and mainstream flows. Data points from the axisymmetric CFD model corroborate the predicted trend with respect to purge swirl velocity. Loss estimates from CFD are somewhat lower due to the fact that the flow is not fully mixed out at the exit of the computational domain.

Looking at Eqn. (4) it is easy to see why mass fraction has an almost linear relationship with shear layer loss (linearity is perturbed due to the fact that for a given gap width, increasing purge mass flow will affect the purge flow velocity terms as well). It is also evident from Fig. 6(a) that swirling purge flow to rim speed brings down losses drastically. However, within the design space spanning $30^\circ < \phi < 90^\circ$ and $4\% < gf < 10\%$ the contour plot of loss coefficient in Fig. 6(b) varies only by about 11%. Note that beyond this design space (particularly for narrow purge gaps, where the purge jet axial and radial kinetic energy

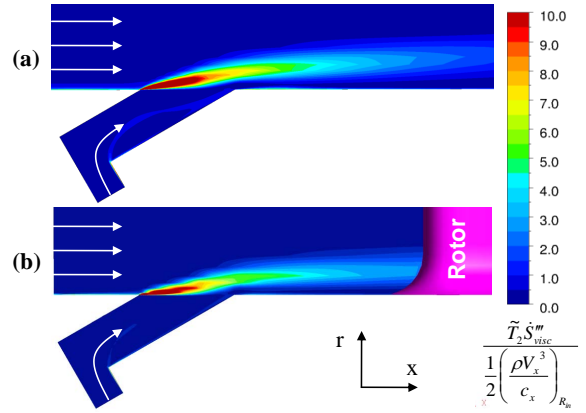


FIGURE 5. VOLUMETRIC ENTROPY GENERATION RATE DUE TO VISCIOUS EFFECTS IN SHEAR LAYER (a)AXISYMMETRIC MODEL(b) THREE DIMENSIONAL ROTOR PASSAGE.

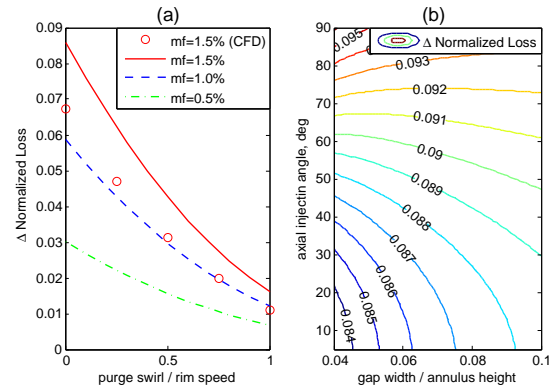


FIGURE 6. PARAMETRIC STUDY OF SHEAR LAYER LOSS USING ANALYTICAL MIXED OUT ANALYSIS. (a)EFFECT OF mf AND sf (b)EFFECT OF gf AND ϕ

become important), the effect of injection angle may become significant, however this would require gap widths much narrower than what is used in current practices. The takeaway message is that mass fraction and swirl are the design parameters with the biggest leverage on shear layer losses.

2. Purge Flow-Passage Vortex Interaction. When purge flow is injected at the hub upstream of a rotor blade, the additional losses incurred usually exceed what would be expected from mixing out of a shear layer. This can be seen in Fig. 7. Figure 7(a) first shows how the losses for the baseline case can be subtracted from a case with purge flow to get the net purge flow-induced loss presented in Fig. 7(b). Figure 7(b) then shows how the loss from the axisymmetric case can be further factored out, leaving the effects of purge flow beyond those related to the

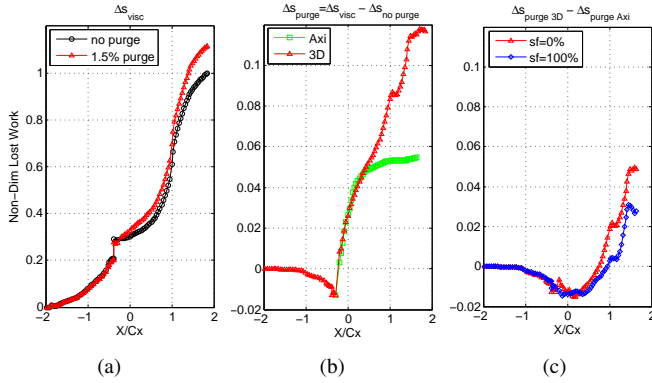


FIGURE 7. ACCUMULATED LOSS (a)THREE DIMENSIONAL STAGE, WITH AND WITHOUT PURGE FLOW (b)NET LOSS DUE TO PURGE FLOW INJECTION FOR AXISYMMETRIC AND 3D STAGE (c)PURGE FLOW LOSSES WITH SHEAR LAYER FACTORED OUT

mixing out of the shear layer. These overhead losses are shown in Fig. 7(c) for two cases - purge flow injected at the hub with and without swirl. We note that there is a reduction in loss through the NGV, but a greater increase in loss in the rotor. Let us first turn our attention to the rotor.

To get a better idea of where the additional losses due to purge flow are being generated within the rotor passage, we refer to Fig. 8, which shows the *change* in volumetric entropy generation rate relative to the baseline case with no purge flow. A region of increased entropy generation rate near the hub upstream of the blade is due to the purge-mainstream shear layer. However there are further increases in entropy generation rate that appear to be related to the passage and tip clearance flow vortices, and even the wetted surfaces exhibit increases in boundary layer losses.

Previous authors [2] [15] [6] [4] have commented on the potential for purge flow to interact with secondary flow structures such as the passage vortex to generate additional losses. Based on Fig. 8, the passage vortex does appear to play a role in generating losses, but we seek a more direct causal relationship.

The kinematics of the secondary flow through the blade passage can be conveyed by the magnitude of the cross-flow velocity, defined in Fig. 9 as the velocity perpendicular to the circumferentially averaged meanline flow direction. For the baseline case with no purge flow injection, there is little cross-flow near the hub up until about 20% axial chord, at which point a distinct cross-flow layer begins to develop below 3% span (Fig. 9(c)) as a consequence of the pressure gradient between suction and pressure side of a turbine blade passage. It has been commonly agreed upon [16] [17] that this cross-flow drives the development of the main passage vortex, the core of which can clearly be discerned near 20% span at the rotor exit plane (Core 1 in Fig. 9(d)). When purge flow is injected without swirl, in the frame of reference of the rotor this purge flow has a strong cross-flow com-

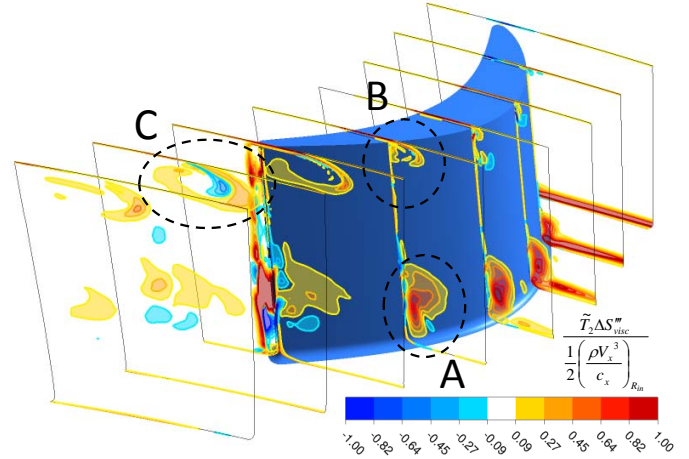


FIGURE 8. CHANGE IN ENTROPY GENERATION RATE PER UNIT VOLUME DUE TO INJECTION OF 1.5% PURGE FLOW AT THE HUB, UPSTREAM OF THE ROTOR

ponent. Consequently, the growth of the cross-flow layer near the endwall is given an early start, reaching a thickness of 5% span by the 20% chord plane (Fig. 9(a-c)). However, the authors observed that the stronger cross-flow resulting from purge flow injection does not lead to a dramatic increase in the main passage vortex, but primarily results in the vortex core being displaced toward the midspan (Core 2 in Fig. 9(d)). This behavior has been observed by a number of other authors [18] [8] [15]. Furthermore, purge flow tends to get entrained in the passage vortex core, which is in accord with results presented in [5] [15] [1] [4].

To link these secondary flow features changes in loss generation near the passage vortex we refer to Figure 10, which shows the volumetric viscous entropy generation rate in the region marked (A) on Fig. 4, superimposed on top of the secondary flow field on that plane ($X/c_x = 0.8$). The first thing to note is that more entropy is being generated due to viscous effects in the *vicinity* of the hub passage vortex when purge flow is injected (Fig. 10(b)), but this effect is mitigated by swirling of the purge flow to rim speed (Fig. 10(c)). A correspondence between the location of the passage vortex and regions of low stagnation pressure has previously led to the hypothesis that the passage vortex cores is the primary source of secondary flow loss ([18] [15] [6]). However, from Fig. 10 it can be seen that the regions of high entropy generation rate do not coincide with the main vortex core, indicating that the vortex itself is not the direct loss-generating mechanism. This observation motivated further investigation into the the root cause of the entropy generation in this region.

It was first necessary to verify that the increase in entropy generation rate near the passage vortex was indeed due to the secondary flow field, and not due to shear in the streamwise di-

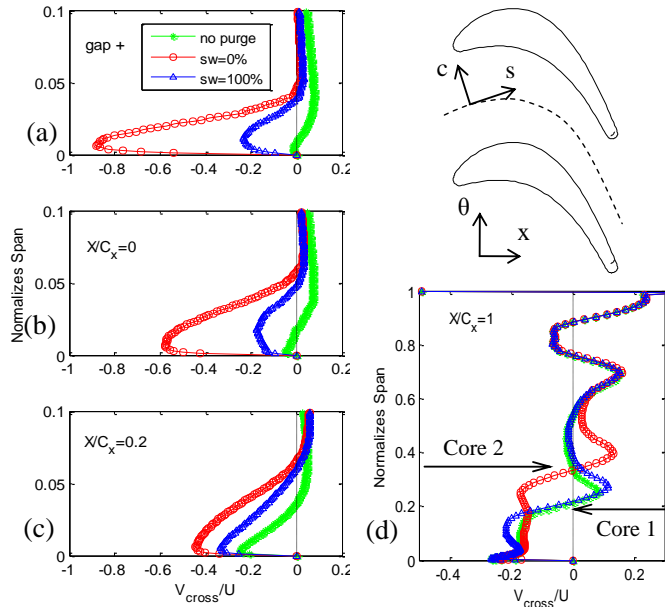


FIGURE 9. CIRCUMFERENTIALLY AVERAGED CROSS-FLOW VELOCITY (a) DOWNSTREAM EDGE OF PURGE SLOT (b-d) 0, 20, 100% AXIAL CHORD

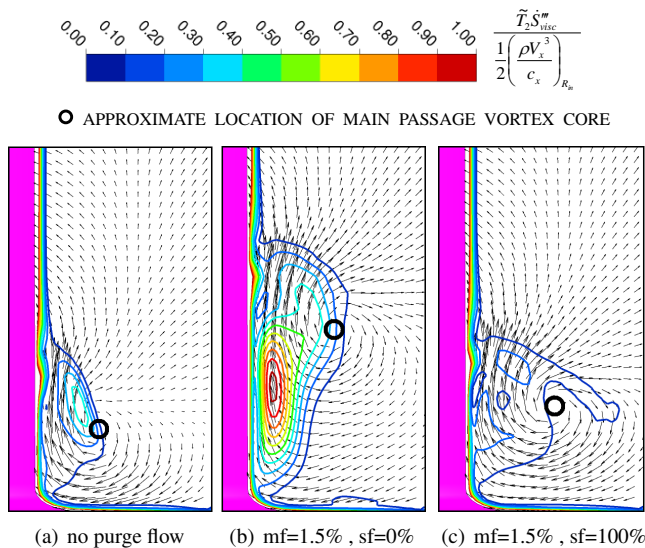


FIGURE 10. ENTROPY GENERATION RATE PER UNIT VOLUME IN REGION (A) OF FIG. 4 IN THE PLANE $X/C_x = 0.8$

rection. For this purpose, we would like to express \dot{S}_{visc}''' in terms of the polar streamline coordinates (s, c, r) defined in Fig. 9, and identify the terms in Eqn. (6) that have the largest contribution. However, because we are dealing with a high hub-to-tip ratio machine ($r_{hub}/r_{tip} = 0.9$) we can work with a set of local Cartesian

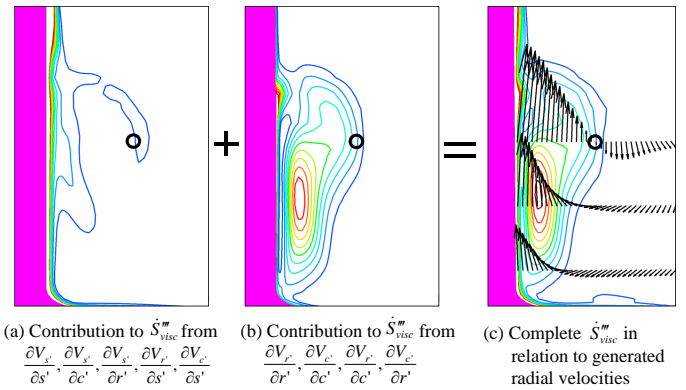


FIGURE 11. DECOMPOSITION OF ENTROPY GENERATION RATE PER UNIT VOLUME IN TERMS OF STREAMWISE TERMS AND SECONDARY FLOW TERMS. LOCATION AND SCALE SAME AS FIG. 10(b)

coordinates (s', c', r') rotated to align with the streamline direction - a close approximation of the polar streamline coordinate system. Expressing \dot{S}_{visc}''' in these rotated Cartesian coordinates, and neglecting compressibility effects (which were verified to be minuscule) results in Eqn. (8)

$$\dot{S}_{visc}''' = \frac{\mu_{eff}}{T} \left\{ 2 \left[\left(\frac{\partial V_{s'}}{\partial s'} \right)^2 + \left(\frac{\partial V_{c'}}{\partial c'} \right)^2 + \left(\frac{\partial V_{r'}}{\partial r'} \right)^2 \right] + \left(\frac{\partial V_{c'}}{\partial c'} + \frac{\partial V_{s'}}{\partial s'} \right)^2 + \left(\frac{\partial V_{r'}}{\partial r'} + \frac{\partial V_{c'}}{\partial c'} \right)^2 \right\} \quad (8)$$

Using this formulation of \dot{S}_{visc}''' we can infer approximate statements regarding the contributions of gradients in V_s, V_c and V_r to entropy generation rates in the passage vortex region. In Fig. 11(a) it is demonstrated that of the terms in Eqn. (8), those involving gradients of streamwise velocity and gradients in the streamwise direction $\left(\frac{\partial V_{s'}}{\partial s'}, \frac{\partial V_{c'}}{\partial r'}, \frac{\partial V_{s'}}{\partial c'}, \frac{\partial V_{r'}}{\partial s'}, \frac{\partial V_{c'}}{\partial s'} \right)$ are dominant in boundary layer losses but have no significant role in generating entropy away from solid surfaces. In contrast, Fig. 11(b) shows that it is the secondary flow terms $\left(\frac{\partial V_{r'}}{\partial r'}, \frac{\partial V_{c'}}{\partial c'}, \frac{\partial V_{r'}}{\partial c'}, \frac{\partial V_{c'}}{\partial r'} \right)$ that generate losses in the vicinity of the passage vortex.

Having demonstrated that the entropy generation is indeed a result of cross-flow and radial-flow terms, a closer look at the secondary flow field in Fig. 11(c) shows that the blade-to-blade cross-flow near the hub is being accelerated through the space between the rotor suction side and the passage vortex. In this respect, the passage vortex serves as a region of blockage, creating the effect of a nozzle that generates high radial velocities. However, the resulting interaction between this radial flow and the passage vortex is not purely a potential flow effect, and shearing occurs between the two flow features. Purge flow injected with no swirl results in a thickened cross-flow layer, as was observed in Fig. 9, creating the conditions for this interaction be-

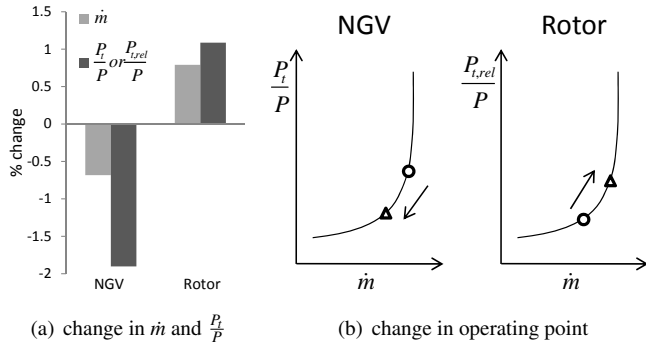


FIGURE 12. CHANGE IN OPERATING POINT FOR NGV AND ROTOR, MF=1.5% SF=0%

tween cross-flow and passage vortex. Both the baseline case and the case with swirled purge flow are subject to the same loss-generating process, but having substantially weaker cross-flows the effect is much diminished.

3. Losses Related to Change in Reaction. As noted in the discussion of Fig. 8, aside from the increased losses in the vicinity of the passage vortex, there are also increases in the entropy generation rate near the blade tip and over most of the wetted surfaces of the rotor passage. The reduction in losses through the NGV, shown in Fig. 7(c) must also be addressed.

The reduction in loss through the NGV has been observed previously in [3], where it was attributed to an increased degree of reaction - a consequence of the blockage introduced with purge flow injection. However, it is important to realize that this change in reaction, while reducing the losses through the NGV, also accounts for some of the increased losses through the rotor. Changes in reaction due to cooling and purge flows are taken into account in the design process², but it is important to be aware of this effect so that one does not mistakenly attribute all of the additional rotor losses in Fig. 7(c) to purge flow-passage vortex interaction.

For the present configuration, injecting 1.5% purge flow increases the degree of reaction from 0.41 to 0.44. Another way of looking at it is that the operating point of both NGV and rotor is shifted as illustrated in Fig. 12, with less acceleration (decreased $\frac{P}{P_0}$) through the NGV but more (increased $\frac{P_{t,rel}}{P}$) through the rotor. The higher pressure drop across the rotor implies a higher pressure difference between the suction and pressure side of the blade, thus leading to more tip clearance flow. In addition, the changes in pressure ratio indicate likewise changes in free stream Mach number, which in turn explains the decreased NGV losses and the higher wetted losses through the rotor. All of these changes are consistent with the observations in Fig. 8.

²Source:David Little, Siemens Energy Inc.

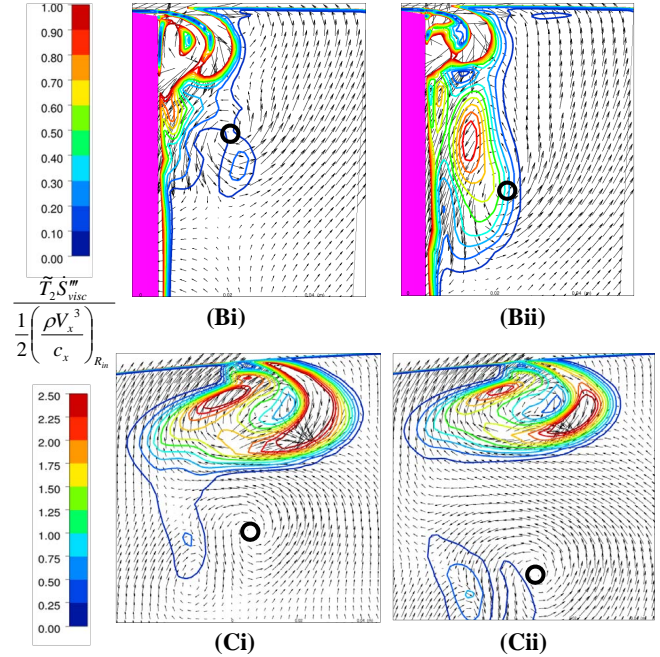


FIGURE 13. ENTROPY GENERATION RATE PER UNIT VOLUME IN REGIONS (B) AND (C) IN FIG. 4 FOR THE BASELINE CASE (Bi,Ci) AND A CASE WITH 1.5% PURGE FLOW INJECTED AT THE SHROUD (Bii, Cii)

To delineate between the change in loss due to purge flow-passage vortex interaction and that due to change in operating point, we make use of the fact that when purge flow is swirled to rim speed there is negligible additional entropy generated due to purge flow-passage vortex interaction, as observed in the entropy generation rate contours of Fig. 10(c). On the other hand, the blockage effect of swirled and non-swirled purge flow is similar since it is primarily a function of purge flow mass fraction. We therefore make the approximation that for the case sf=100%, all losses beyond those due to the shear layer are due to a change in reaction. The difference between sf=0% and sf=100% is then attributed entirely to purge flow-passage vortex interaction. Figure 7(c) illustrates this method of delineation.

4. Purge-Tip Clearance Flow Interaction. When purge flow is injected from the shroud upstream of the un-shrouded rotor, some of the effects are similar to the case of hub-injection, while other effects differ. Losses due to purge-mainstream shear layer are similar to those for hub-injected purge flow. In terms of secondary flow effects, Fig. 13 shows a close-up of the regions marked (B) and (C) in Fig. 4 for the cases with and without purge flow. Comparison between (Bi) and (Bii) demonstrates the migration of the passage vortex towards the midspan (passage vortex core is marked with a black

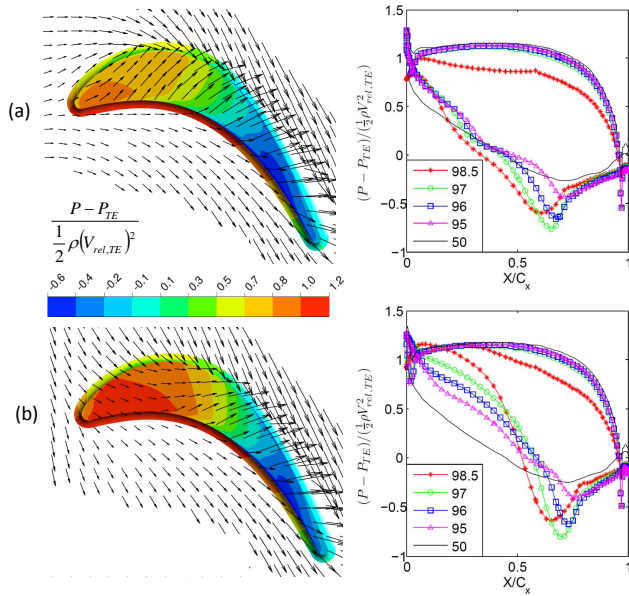


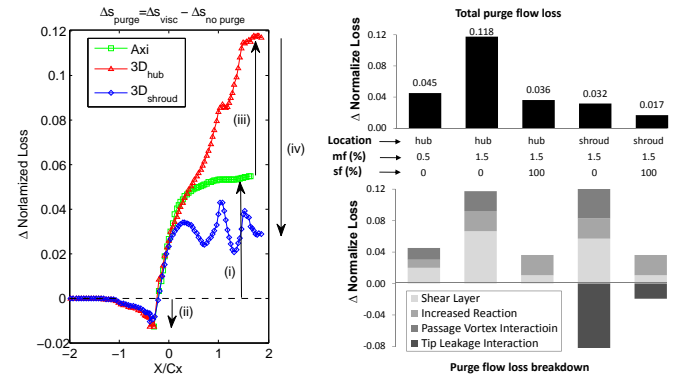
FIGURE 14. VELOCITY FIELD IN ROTOR FRAME OF REFERENCE HALF WAY BETWEEN ROTOR TIP AND SHROUD, AND BLADE LOADING AT 95,96,97,98.5 AND 50% SPAN a)NO PURGE b)1.5% PURGE FLOW AT SHROUD

circle), and the accompanying increase in purge flow-passage vortex losses. In these respects the effects of shroud injected purge flow are similar to hub injected purge flow. However, despite an increased degree of reaction, tip clearance flow loss has decreased dramatically. This reduction can be seen most clearly downstream of the blade where most the tip clearance flow losses are realized, in (Ci) and (Cii) of Fig 13.

This reduction in tip clearance loss can be explained once again by thinking in terms of the cross-flow introduced in the shroud region due to the non-swirled purge flow’s relative motion in the rotating frame. Figure 14 shows the vector field in a plane halfway between the rotor tip gap, for a case with and without purge flow. The case in Fig. 14(b) clearly shows how the tangential momentum of the purge flow suppresses tip clearance flow in the forward part of the blade. This is also reflected in the blade loading distribution of the top 5% span (also shown in Fig. 14), as the negative incidence of the purge flow has reduced the pressure difference across the front part of the blade, and hence reduced the driving force for leakage flow across the tip clearance.

Quantitative Analysis of Design Effects

A method for delineating the loss mechanisms associated with purge flow injection in quantitative terms is illustrated in Fig. 15(a). The procedure is as follows: Shear layer loss is taken from the axisymmetric results (labeled ‘i’ in Fig. 15(a)). Purge



(a) Additional viscous loss due to purge flow injection

(b) Total purge flow losses and loss breakdown for various cases

FIGURE 15. PROCEDURE FOR ISOLATING AND COMPARING PURGE FLOW LOSS MECHANISMS. LOSSES NORMALIZED BY BASE-LINE STAGE LOSSES

flow losses beyond those found in the axisymmetric case (i and iii) are due to the combined effect of purge flow-passage vortex interaction and change in operating point. As discussed, the fraction of these additional losses caused by changes in the operating point is based on the losses for a case with $sf=100\%$, and the remaining purge flow-passage vortex interaction loss is obtained by comparing $sf=100\%$ and $sf=0\%$. The tip clearance flow suppression effect with shroud-injected purge flow is quantified by assuming that all other losses are the same as for hub injection, and any difference in the losses between cases of hub and shroud-injection is due to tip clearance flow suppression(iv).

Figure 15(b) shows the overall change in loss due to purge flow, as well as the breakdown of the various purge flow-related loss mechanisms, for a number of configurations that had a significant impact on purge flow losses. Mass fraction, as expected, is a strong controlling parameter, leading to an almost 12% increase in loss relative to the baseline for $mf=1.5\%$. However swirling this purge flow to rim speed reduces these losses by more than 2/3. Note, however, that in the case of shroud injected purge flow, total purge flow losses are not that severe to begin with due to the tip clearance flow suppression effect. On the other hand, swirling shroud-injected purge flow affords little further reduction in loss, since there is a tradeoff with the tip clearance flow suppression effect.

Gap fraction and injection angle were found to be of secondary importance, demonstrating less than 6% reduction in purge flow losses over the entire design space. In the first place this is due to the fact that these are control parameters affecting the shear layer loss only, which is responsible for 1/2 of the turbine losses. Furthermore, it was shown in Fig. 6 that the shear layer loss is dominated by the circumferential velocity deficit between purge and mainstream, rather than the axial and radial

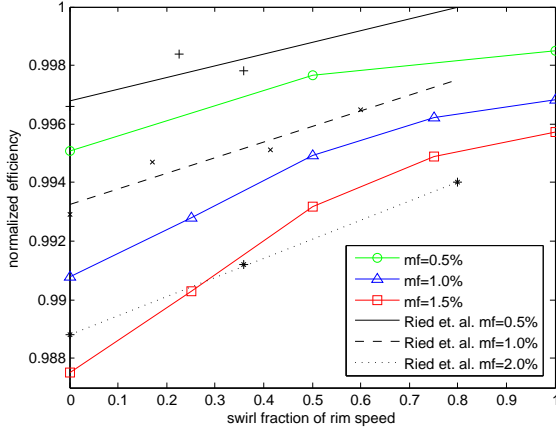


FIGURE 16. COMPARISON OF PRESENT RESULTS TO EXPERIMENTAL DATA PUBLISHED BY REID ET. AL. [3]

components that are determined by ϕ and gf .

Although the present study does not include validation of computational results through experiment, there is reasonable agreement between our findings and published data in the literature. Figure 16 shows normalized efficiency trends with purge swirl velocity and mass fraction, as compared to experimental data published in [3]. The results from the present study yield a quadratic relationship of loss and swirl fraction. This is not surprising, as the shear layer loss was shown analytically to be a quadratic function of purge swirl velocity in Eqn. (4). On the other hand, the experimental data of Reid et. al. suggests a linear trend in efficiency improvement with swirl fraction. This is likely because in a physical scenario purge flow tends to pick up swirl due to windage as it travels through rim seals, particularly at low swirl fractions (when the relative motion between purge flow and rotating seal walls is highest). At higher swirl fractions, when this phenomena is less pronounced, the present results are in reasonable accord with the experimental results of Reid et. al. Since non-swirled purge flow is never really the case, a more realistic assessment of the potential for reducing purge flow losses through an intentional swirling device would be the comparison of $sf=50\%$ vs. $sf=100\%$, in which case the higher swirl reduces the purge flow losses per unit mass injected by 40%.

The present results are also reasonably consistent with the numerical investigation of Ong et. al. [4]. In that study, the authors found a 0.75%-point increase in efficiency when going from $mf=0.84\%$ $sf=0\%$ to $mf=0.69\%$ $sf=110\%$ (the mass flow was not kept constant between the swirled and non-swirled cases in that study). Of this improvement it was estimated that 0.4%-points are due to reductions in shear layer loss, and the remaining 0.35%-points are due to correction of the negative incidence due of purge flow - a similar breakdown to what was found in the present results. Interpolating from the results of the present work

would give an improvement of about 0.55%-point. Although the numbers do not agree perfectly, most of our qualitative observations, in terms of secondary flow kinematics and drivers for loss, are consistent. Ong et. al. [4] also establishes a link between negative incidence of purge flow and reduced work extraction in the turbine, through use of the Euler Turbine Equation, but this reduction of work output is not necessarily due to loss, but rather due to a change in w_{ideal} . By looking at the problem in the context of entropy generation sources and drivers for high shear strain rate we have added new insight into how loss generation in a turbine flow path comes about as a result of purge flow injection.

SUMMARY

A consistent framework for interpreting turbine losses is presented, in which it is shown that entropy production due to thermal mixing should be considered a cycle loss and only viscous losses constitute a debit to turbine performance. A method for isolating and tracing viscous entropy generation sources is presented in the form of accumulated loss curves and volumetric entropy generation rate. These tools were used to identify four effects through which purge flow affects turbine losses, and these are summarized in Table 2. A method for delineating the contributions of these effects is presented in the form of systematic factoring out of the different effects.

TABLE 2. SUMMARY OF THE EFFECTS PURGE FLOW HAS ON LOSS

Effect	Drivers and traceability of loss generation
Shear layer	Purge-mainstream velocity deficit, primarily ΔV_{θ} , leads to viscous shear
Passage vortex interaction	Non-swirled purge flow thickens cross-flow layer. Passage vortex acts as blockage, forcing cross-flow up the suction side of the blade and generating high radial velocities. Shearing occurs between this radial flow and the passage vortex.
Increased Reaction	Purge flow blockage decreases $\frac{P}{P}$, \dot{m} , M and wetted loss through NGV, but increases $\frac{P_{t,rel}}{P}$, \dot{m} , M_{rel} and wetted + tip clearance losses through rotor.
Tip clearance flow interaction	Tangential momentum of purge flow in the relative frame suppresses tip clearance flow in the forward part of the blade

CONCLUSION

Purge air injection can increase turbine losses by 12% when 1.5% purge flow is introduced at the hub. About 1/2 of this loss is

due to the shear layer between mainstream and purge flow, while the remaining 1/2 is due to a higher wetted and tip clearance flow losses and interaction between a thickened cross-flow layer near the hub and the passage vortex system. When purge flow is injected at the shroud it has the beneficial effect of suppressing tip-clearance flow, thereby offsetting 3/4 of the increased viscous losses due its injection. Given the understanding gained through a systematic delineation of these loss mechanisms and their drivers it was possible to rationalize the sensitivity of loss to a number of design parameters: Mass fraction of purge flow is the parameter with the highest leverage on purge flow losses, since it has a close to linear relationship with all of the purge flow loss mechanisms. The magnitude of purge air swirl velocity has the potential of reducing purge flow losses by 40-70%. On the other hand, for the design space under consideration, purge gap width and injection angle have limited ability in affecting only the shear layer loss mechanism, which itself accounts for only 1/2 of the turbine losses. Finally, by taking into account the change in operating point resulting from purge flow injection, it is possible to design against excessive tip clearanec flow and wetted losses.

ACKNOWLEDGMENT

The authors would like to express their thanks to Manoj Singh, for his hard work in providing many of the CFD results, Dave Little and Barry Brown for providing insight into industry practices, and Professor Nick Cumpsty, for the illuminating discussions that helped guide our research. CFX and TecPlot support staff have been kind in providing assistance with CFD and post processing issues. We are also grateful to the reviewers of this paper for helping us bring clarity to our presentation. This program was supported by MITEI Sustaining Member Siemens CKI, agreement dated 09/30/08.

PERMISSION FOR USE:

The content of this paper is copyrighted by Siemens Energy, Inc. and is licensed to ASME for publication and distribution only. Any inquiries regarding permission to use the content of this paper, in whole or in part, for any purpose must be addressed to Siemens Energy, Inc. directly.

REFERENCES

[1] Pau, M., Paniagua, G., Delhaye, D., la Loma de, and Gini-bre, P., 2010. "Aerothermal impact of stator-rim purge flow and rotor-platform film cooling on a transonic turbine stage". *ASME Journal of Turbomachinery*, **132**, 021006.
 [2] Kost, F., and Nicklas, M., 2001. "Film-cooled turbine end-wall in a transonic flow field: Part i - aerodynamic mea-

surements". *ASME Journal of Turbomachinery*, **123**(4), pp. 709–719.
 [3] Reid, K., Denton, J., Pullan, G., Curtis, E., and Longley, J., 2006. "The effect of stator-rotor hub sealing flow on the mainstream aerodynamics of a turbine". In 2006 ASME 51st Turbo Expo, May 6, 2006 - May 11, Vol. 6 PART A, American Society of Mechanical Engineers, pp. 789–798.
 [4] Ong, J. H. P., Miller, R. J., and Uchida, S., 2006. "The effect of coolant injection on the endwall flow of a high pressure turbine". In 2006 ASME Turbo Expo, Vol. 6, American Society of Mechanical Engineers, pp. 915–924, GT2006–91060.
 [5] Popovi, I., and Hodson, H. P., 2010. "Aerothermal impact of the interaction between hub leakage and mainstream flows in highly-loaded hp turbine blades". *Proceedings of ASME Turbo Expo 2010: Power for Land, Sea and Air*, June 14-18, 2010.
 [6] de la Rosa Blanco, E., Hodson, H. P., and Vazquez, R., 2006. "Effect of the leakage flows and the upstream platform geometry on the endwall flows of a turbine cascade". In 2006 ASME 51st Turbo Expo, May 6, 2006 - May 11, Vol. 6 PART A, American Society of Mechanical Engineers, pp. 733–744.
 [7] S., Vlastic, E., Lavoie, J. P., and Moustapha, S. H., 2002. "The effect of secondary air injection on the performance of a transonic turbine stage". In Proceedings of the ASME TURBO EXPO 2002: Turbomachinery, June 3, 2002 - June 6, Vol. 5 A, American Society of Mechanical Engineers, pp. 147–157.
 [8] McLean, C., Camci, C., and Glezer, B., 2001. "Mainstream aerodynamic effects due to wheelspace coolant injection in a high-pressure turbine stage: Part i - aerodynamic measurements in the stationary frame". *ASME Journal of Turbomachinery*, **123**(4), pp. 687–696.
 [9] Young, J. B., and Wilcock, R. C., 2002. "Modeling the air-cooled gas turbine: Part 2-coolant flows and losses". *ASME Journal of Turbomachinery*, **124**(2), pp. 214–221.
 [10] Cumpsty, N. A., and Horlock, J. H., 2006. "Averaging nonuniform flow for a purpose". *ASME Journal of Turbomachinery*, **128**(1), pp. 120–129.
 [11] Young, J. B., and Horlock, J. H., 2006. "Defining the efficiency of a cooled turbine". *Transactions of the ASME. The Journal of Turbomachinery*, **128**(4), 10, pp. 658–67.
 [12] Horlock, J. H., 2001. "The basic thermodynamics of turbine cooling". *ASME Journal of Turbomachinery*, **123**(3), pp. 583–592.
 [13] Young, J. B., and Wilcock, R. C., 2002. "Modeling the air-cooled gas turbine: Part 1-general thermodynamics". *ASME Journal of Turbomachinery*, **124**(2), pp. 207–213.
 [14] Greitzer, E. M., Tan, C. S., and Graf, M. B., 2004. *Internal Flow*. Cambridge University Press., New York, NY.

- [15] Paniagua, G., Denos, R., and Almeida, S., 2004. “Effect of the hub endwall cavity flow on the flow-field of a transonic high-pressure turbine”. *ASME Journal of Turbomachinery*, **126**(4), pp. 578–586.
- [16] Sharma, O. P., and Butler, T. L., 1987. “Predictions of endwall losses and secondary flows in axial flow turbine cascades”. *ASME Journal of Turbomachinery*, **109**(2), pp. 229–236.
- [17] Wang, H.-P., Olson, S. J., Goldstein, R. J., and Eckert, E. R. G., 1995. “Flow visualization in a linear turbine cascade of high performance turbine blades”. In Proceedings of the International Gas Turbine and Aeroengine Congress and Exposition, June 5, 1995 - June 8, ASME, pp. 11–11pp.
- [18] Schuler, P., Kurz, W., Dullenkopf, K., and Bauer, H. J., 2010. “The influence of different rim seal geometries on hot-gas ingestion and total pressure loss in a low-pressure turbine”. *Proceedings of ASME Turbo Expo 2010: Power for Land, Sea and Air*, June 14–18, 2010,.

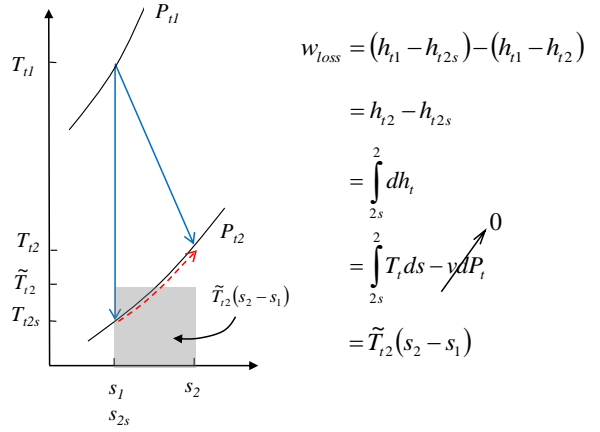


FIGURE 17. LOST WORK IN TURBINE EXPANSION

Appendix A: Entropy as a Measure of Loss

The first and second laws of thermodynamics are given for a differential process by Eqn (9) and Eqn (10).

$$\delta w = \delta q - dh \quad (9)$$

$$ds = \frac{\delta q}{T} + ds_{irrev} \quad (10)$$

Combining the two to eliminate the heat transfer term yields an expression for the work extracted for a reversible ($ds_{irrev} = 0$) and non-reversible process, given by Eqn. (11) and Eqn. (12) respectively.

$$\delta w_{rev} = -dh + T ds \quad (11)$$

$$\delta w = -dh + T ds - T ds_{irrev} \quad (12)$$

The difference between the two processes gives the lost opportunity to do work, which is given by Eqn. (13). Therefore, entropy generation due to irreversible processes is a fundamental measure of lost opportunity to do work.

$$\delta w_{loss} = \delta w_{rev} - \delta w = T ds_{irrev} \quad (13)$$

For an expansion through a turbine, one can go through the process outlined in Fig. 17 to derive an effective temperature at which entropy is generated, \tilde{T}_{t2} . This temperature is an average of T_{t2} and T_{t2s} , but choosing either one will give minuscule error when calculating dissipation.

Appendix B: Delineation of Baseline Loss Mechanisms

The losses for the baseline case with no purge flow can be delineated in the following way:

1. Profile loss is calculated by the change in entropy at midspan (away from secondary flows and endwall boundary layers)
2. Endwall wetted loss is calculated using a constant dissipation coefficient of 0.002 and the local velocity-cubed relationship given in [10]
3. Tip clearance loss was calculated by subtracting the losses from a case with no tip clearance gap from the total baseline losses. (a fillet was added to the shroud for the case of no tip clearance to minimize any corner vortex losses)
4. Baseline secondary flow loss (which includes losses due to all vortical structures) is calculated as the remainder of the loss after subtracting out the profile, endwall and tip clearance losses.